UC Santa Barbara
UC Santa Barbara Previously Published Works

Title

Light-activated RNA interference in human embryonic stem cells

Permalink

https://escholarship.org/uc/item/8sg1g5hd

Authors

Huang, Xiao
Hu, Qirui
Braun, Gary B
et al.

Publication Date

DOI

Peer reviewed

CrossMark

Light-activated RNA interference in human embryonic stem cells

Xiao Huang [a], Qirui Hu [b], Gary B. Braun [c], Alessia Pallaoro [a], Demosthenes P. Morales [a],
Joseph Zasadzinski [d], Dennis O. Clegg [b], Norbert O. Reich [a, *]

[a] Department of Chemistry and Biochemistry, University of California, Santa Barbara, CA 93106, United States
[b] Center for Stem Cell Biology and Engineering, University of California, Santa Barbara, CA 93106, United States
[c] Cancer Research Center, Sanford-Burnham Medical Research Institute, La Jolla, CA 92037, United States
[d] Department of Chemical Engineering and Materials Science, University of Minnesota, Minneapolis, MN 55455, United States

ARTICLE INFO

ABSTRACT

We describe a near infrared (NIR) light-activated gene silencing method in undifferentiated human embryonic stem cell (hESC) using a plasmonic hollow gold nanoshell (HGN) as the siRNA carrier. Our modular biotin-streptavidin coupling strategy enables positively charged TAT-peptide to coat oligonucleotides-saturated nanoparticles as a stable colloid formation. TAT-peptide coated nanoparticles with dense siRNA loading show efficient penetration into a wide variety of hESC cell lines. The siRNA is freed from the nanoparticles and delivered to the cytosol by femtosecond pulses of NIR light with potentially exquisite spatial and temporal control. The effectiveness of this approach is shown by targeting *GFP* and *Oct4* genes in undifferentiated hESC (H9). The accelerated expression of differentiation markers for all three germ layers resulting from *Oct4* knockdown confirms that this method has no detectable adverse effects that limit the range of differentiation. This biocompatible and NIR laser-activated patterning method makes possible single cell resolution of siRNA delivery for diverse studies in stem cell biology, tissue engineering and regenerative medicine.

Published by Elsevier Ltd.

1. Introduction

The capability of human embryonic stem cells (hESC) differentiation into all types of cells in the body holds immense promise in tissue engineering and regenerative medicine [1–3], and is of interest for generating disease models for drug screening. RNA interference (RNAi) has been a powerful tool to dissect genetic pathways and manipulate cellular phenotypes [4–9]. However, the routine use of RNAi in stem cells requires efficient and biocompatible delivery methods [10–12], and while the commonly used viral-based RNAi methods are efficient [13,14], these can be time-consuming and pose substantial biosafety problems, such as risk of secondary infection and immunogenic response [15–17]. Commercially available transfection reagents such as Lipofectamine have had some success in hESC transfection [9,18,19]. However, lipofectamine use could result in unacceptable levels of cytotoxicity and nonspecific changes in gene expression [11,19–21]. Alternative chemical transient transfection methods using nanocarriers of cationic lipids, polymers, and functionalized gold nanoparticles have also had variable success with hESC derivatives including embryoid bodies, human mesenchymal stem cells and neural stem cells [8,10,11,22–27], but transfection of undifferentiated hESC remains a challenge for synthetic vectors. Importantly, specific targeting within populations of similar cells is not possible using current methods. To address these needs, we have developed an efficient, biocompatible and broadly applicable method to introduce siRNA into hESC by near infrared light-controlled endosome rupture. This delivery method provides i) efficient endosome escape, ii) control over the timing of siRNA delivery to the cytosol, iii) individual cell-level resolution, and iv) minimal toxicity. Applications include self-renewal studies of undifferentiated stem cells and tissue engineering — an area with pressing need for new technologies for efficient and cell-specific RNAi delivery [28,29]. For example, this light-responsive RNAi release strategy has the ability to load different types of RNAi on the nanocarriers with distinct absorption spectrum [30] and activate specific RNAi in the required regions of cells by light irradiation at corresponding wavelength, which can cause the directed differentiation of stem cells to different cell types in a spatially organized pattern during early embryogenesis such as optic cup formation for ocular development

---

* Corresponding author.
 E-mail address: reich@chem.ucsb.edu (N.O. Reich).

[31,32], Rathke's pouch formation for pituitary tissue development [33] and tooth-germ structure for tooth growth [34].

To create the light-activated hESC silencing system, siRNA molecules were first densely assembled onto plasmonic hollow gold nanoshells (HGN) via thiol bond formation, then were overcoated with a protective protein layer with handles for attaching cell penetrating peptides [35,36]. Upon irradiation with biocompatible near infrared (NIR) light (~800 nm), the siRNAs are released from the gold surface (due to carrier surface specific thiol—gold bond dissociation). Endosomal rupture results from vapor layer formation around the hot gold nanoparticles [37]. In this work, we explored the ability of HIV-derived cell penetrating peptide (CPP) TAT (YGRKKRRQRRR) to facilitate the internalization of the HGNs into hESC. However, direct conjugation of TAT-peptide and siRNA-conjugated HGNs resulted in aggregation, presumably due to colloidal surface charge neutralization and bridging between the cationic TAT and the anionic siRNA [38,39]. We devised an alternative surface coating strategy by positioning TAT on the siRNA via coupling with the tetravalent protein streptavidin, which sterically prevents the siRNA from electrostatic contacts and thus inhibits particle aggregation. The resulting construct (Fig. 1a) was capable of releasing siRNA payloads upon NIR laser irradiation and could efficiently internalize into a variety of hESC cell lines.

We optimized the knockdown and viability of hESC through a series of protocol variations including cellular dissociation, NIR laser intensity modulation, and ROCK inhibition. To demonstrate the general feasibility of this approach and light-dependent knockdown control, we silenced GFP in engineered H9 cells, and Oct4 in the original H9 cells. Based on the work described here and our prior work, we anticipate spatio-temporal control with siRNA to provide a powerful new avenue for basic research in stem cells and tissue engineering.

2. Materials and methods

2.1. Cell culture

The human embryonic stem cells H1, H7, H9 and H14 (WiCell Research Institute) were maintained on Matrigel (BD Biosciences) coated 6-well plates (BD Falcon) with mTeSR1 medium (Stem Cell Technologies) at 37 °C in 5% CO_2. Cells were passaged by manual dissection without enzymatic dissociation every 5—7 days. For differentiation, H9 cells were cultured with differentiation medium (Dulbecco's modified Eagle's medium (DMEM)/F12, 20% knockout serum replacement, 0.1 mM MEM nonessential amino acid solution, and 0.1 mM β-mercaptoethanol (all from Invitrogen)). HEK293T cells (CRL-11268) were maintained in DMEM supplemented with 10% fetal bovine serum. 50 μg/mL Normocin (InvivoGen) was supplemented in cell culture media.

2.2. Lentiviral transfection to generate transduced H9-GFP and knockdown Oct4 gene expression

The generation of transduced H9-GFP cell line and the knockdown of Oct4 gene through lentiviral transfection are described in the Supplementary Material.

2.3. siRNA transfection with commercial transfection reagents

The protocol for testing commercially available transfection reagents Lipofectamine 2000 (Invitrogen), Lipofectamine RNAiMAX (Invitrogen) and jetPRIME (Polyplus-transfection Inc.) in transduced H9-GFP cells is described in the Supplementary Material.

2.4. Hollow gold nanoshell synthesis, characterization and dsDNA/siRNA assembly

The protocols for HGN synthesis and oligonucleotides (Supplementary Table 1) assembly are described in the Supplementary Material.

2.5. TAT-peptide coating on HGN-dsDNA/siRNA

A large excess (~1.5 mg/mL) of NHS-PEG₄-Biotin (Thermo SCIENTIFIC, #21362) dissolved in 50 μL DMSO was added to 1 mL—0.1 nM HGN-dsDNA or siRNA to functionalize the 3′ end of thiol-DNA or -RNA with biotin. The solution was sonicated briefly and incubated for 1 h at RT, followed by washing with conjugation wash buffer twice to remove excess functionalizing reagent. All the nanoparticle washing steps were performed by centrifuging at ~7000 × g for 10 min and resuspending the pellet in the respective buffer outlined below through brief sonication. Streptavidin (PROzyme) was then coated on biotinylated oligonucleotides on HGN to bridge between nucleic acid and biotinylated TAT-peptide, by adding at 1 mg/mL to ~0.05 nM nanoparticle in the presence of 0.5 × PBST (DPBS with 0.1% Tween-20) and incubating at RT for 1 h after brief sonication. To avoid the particle self-aggregation that may be caused by streptavidin bridging, the solution was vortexed and sonicated immediately upon the addition of streptavidin. The sequential washing of particles with two kinds of buffer (assembly washing buffer and conjugation washing buffer) enhanced the nanoparticle monodispersity. HGN-dsDNA or siRNA with streptavidin coating was finally coated with biotin-TAT (N-terminal biotin, YGRKKRRQRRR, C-terminus free GenScript) to form the multivalent TAT-peptide layer on the outside, of which biotin-TAT was added to ~0.05 nM nanoparticle twice at 15 μM in the presence of 0.5 × PBST followed by brief sonication and 30 min incubation at RT. The nanoparticles were then sequentially washed with assembly washing buffer and conjugation washing buffer again, and concentrated to ~0.3 nM by centrifugation at ~7000 × g for 10 min and the pellet was resuspended in conjugation wash buffer. Particles with nucleic acid and TAT-peptide coating were stored at 4 °C prior to adding to cells.

2.6. Particle transfection and femtosecond laser irradiation

hESC including H1 (passage 38—40), H7 (passage 40—42), H9 (passage 60—70), and H14 (passage 66—68) on 6-well plates were dissociated by rinsing and incubating with 500 μL PBS (Ca^{2+} and Mg^{2+} free, Invitrogen #10010-023) at 37 °C in 5% CO_2 atmosphere for 10 min followed by manual dissection to suspend the cells. The suspended cell aggregates solution was added to 1 mL mTeSR1+10%FBS and pipetted gently with a P1000 pipette for 10—15 times to further decrease the size of the cell aggregates Thereafter, cells in the format of single cell or small cell aggregates (5—10 cells per aggregate) were centrifuged at 145 × g and resuspended in mTeSR1+10%FBS at ~2 × 10⁶ cells/mL. 13 pM of coated particles (after brief sonication) were added to 200 μL of cell suspension and incubated in 1.5 mL Eppendorf tubes at 37 °C for 2 h, with gentle pipetting of the solution by P1000 pipette for 5 times every 30 min. Cells were washed by adding 1.2 mL cold PBS, centrifuging at 55 × g for 3 min and resuspending in 45 μL cold PBS. Tubes with ~50 μL of cell suspension were irradiated with 2.4 W/cm² pulsed NIR laser for 15 s by the output of a femtosecond Ti:sapphire regenerative amplifier (Spectraphysics Spitfire) with the same setup as previously described [35,36]. The laser beam diameter was ~4 mm with the spectral range of 800 ± 6 nm, and the pulse duration was ~130 fs with the repetition rate at 1 kHz. The cells were either used for fluorescence intensity measurements by flow cytometry or plated in Matrigel-coated 12-well plates (~2 × 10⁵ cells per well) in the presence of 10 μM ROCK inhibitor over the first 24 h.
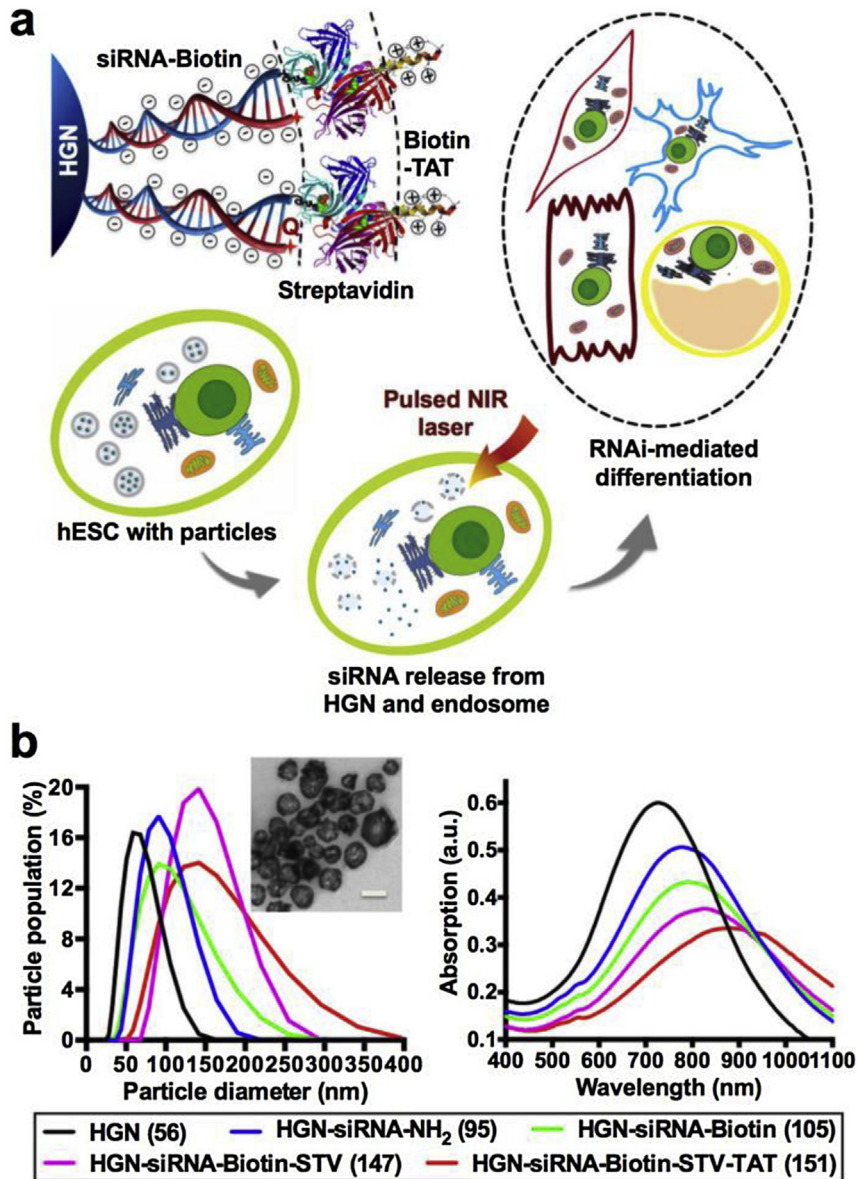
Fig. 1. Nanoparticle architecture and characterization of siRNA on HGN, and schematic of nanoparticle uptake, NIR laser-activated siRNA delivery and RNAi-mediated differentiation in hESC. (a) Schematic of the HGN-siRNA-TAT architecture, NIR laser-activated siRNA delivery and RNAi-mediated differentiation in hESC. Q: Quasar570. (b) Size distribution and absorption spectra of nanoparticles during the coating steps. HGN-citrate has a Z-average diameter of 56 nm; HGN-siRNA-NH$_2$, 95 nm; HGN-siRNA-Biotin, 105 nm; HGN-siRNA-Biotin-STV, 147 nm; and final construct HGN-siRNA-Biotin-STV-TAT, 151 nm. Upper right of the left panel: TEM image of the final construct. Scale bar: 50 nm.

2.7. Imaging of particles in cells

hESC were dissociated into single cells and small aggregates by PBS treatment as described above followed by seeding on a Matrigel-coated 4-well chamber Permanox slide (Lab-Tek #70400) (~4 × 10^4 cells per well) in the presence of 10 μM ROCK inhibitor. The next day, coated nanoparticles were added at 13 pM after the medium switch to mTeSR1+10%FBS, and cells were incubated at 37 °C in 5% CO$_2$ atmosphere for 2 h. After that, cells were washed in PBS twice, fixed in 4% paraformaldehyde (PFA) (VWR International, LLC) in PBS, and washed in PBS again. Cell nuclei were stained using Hoechst 33342 (Sigma−Aldrich). Samples were mounted with Gel/ Mount (Electron Microscopy Science) and visualized under light and fluorescence microscopy. Dark-field scattering images were recorded using an Olympus BX51 upright microscope with a reflection-mode high numerical aperture darkfield condenser

(U-DCW, 1.2−1.4). A 100 × /1.30 oil Iris objective (UPLANFL) was used to collect only the scattered light from the samples. Images were recorded using a QImaging Retiga-2000R Fast 1394 camera with RGB color filter module, while fluorescence images were taken under the mono module. Laser scanning confocal microscopy was performed using an Olympus Fluoview 1000, with 405 nm and 559 nm lasers under the presets of DAPI (blue) and Quasar570 (red), in sequential linescan mode. 24 slices in Z-stack with 0.4 μm increments were obtained from a single cell scan, and images were then digitally assembled using Imaris software to generate the 3D reconstruction image of cells.

2.8. Flow cytometry analysis

Fluorescence intensity of GFP expression and the immunocytochemistry staining levels of OCT4, SSEA and TRA-1-60 were

measured using a BD Accuri C6 flow cytometer with a flow rate of 14 μL/min. Quantification of the particle internalization was achieved through flow cytometry fluorescence measurement of Quasar570. The gate was based on the lineage range of forward and side scattering plots, and 10,000 gated events were collected for each sample. To assay particle internalization from Quasar570 and GFP expression, cells were dissociated into single cells with Accutase (Life Technologies) and collected to inject into the flow cytometer for analysis. OCT4, SSEA4 and TRA-1-60 protein quantification was performed by collecting cells in suspension and staining through immunocytochemistry as follows: cells were fixed in 4% PFA in PBS (4 °C, 20 min) after the dissociation of cells using Accutase. For OCT4 immunocytochemical staining, additional cell permeabilization was performed in 0.2% Triton-X-100 (Sigma−Aldrich) with 0.1% bovine serum albumin (BSA) (Sigma−Aldrich) for 3 min. After washing in PBS with 0.5% BSA, approximately 200 μL of cell suspension containing 2×10^5 cells were incubated with primary antibodies OCT4 (Santa Cruz Biotechnology #sc-5279), SSEA4 (Millipore #MAB4304), and TRA-1-60 (Millipore #MAB4360) for 30 min at RT. Cells were then collected by centrifugation, washed in 0.5% BSA and incubated with secondary antibody Alexa Fluor 488 Goat-anti-Mouse IgG, IgM (H + L) (Invitrogen A10680) for 30 min at RT. Finally, cells were washed, resuspended in 200 μL PBS, and injected in the flow cytometer for analysis.

2.9. Immunocytochemistry of attached cells

Attached cells in culture were washed with PBS, fixed with 4% PFA in PBS (4 °C, 20 min) and washed with PBS again. Cells were then permeabilized by incubating with the blocking solution [1% Goat Serum (Invitrogen) + 1% BSA (Sigma−Aldrich) + 0.1% NP40 (Sigma−Aldrich)] for 1 h at RT. Thereafter, cells were incubated with primary antibodies OCT4, βIII-tubulin (Sigma #T8660), α-smooth muscle actin (Sigma #A5228) and α-fetoprotein (Santa Cruz Biotechnology #sc-166325) diluted in the blocking solution for 1 h at RT. After three PBS washes, all samples were incubated with secondary antibody Alexa Fluor 488 Goat-anti-Mouse IgG, IgM (H + L) diluted in the blocking solution for 1 h at RT. Following the nuclei staining using Hoechst 33342, cells were imaged with an Olympus IX70 inverted microscope.

2.10. Cell viability assay

The effect of particle internalization and NIR laser treatment to stem cell viability was assayed by cell coverage in wells after culturing the treated cells in plates. The treated or untreated control cells were seeded on Matrigel-coated 12-well plate at 2×10^5 cells per well and cultured using mTeSR1 medium for 5 days (in the presence of 10 μM ROCK inhibitor in the first 24 h). After washing with cold PBS twice, cells were stained with crystal violet (Sigma−Aldrich) solution (1% in PBS) for 10 min, followed an additional four washes with PBS. Only the area covered by cells was stained. The wells were imaged by a digital camera and the stained areas in the images were analyzed using ImageJ software.

2.11. Western blotting

The protocol for Western blotting to test the OCT4 protein expression is described in the Supplementary Material.

2.12. Reverse transcription PCR

Total cell RNA was extracted using RNeasy Mini Kit (QIAGEN #74104) according to the manufacturer's instructions, and RNase-Free DNase Set (QIAGEN #79254) was used to remove genomic DNA contamination during the extraction. ~1 μg total RNA from each sample was subjected to reverse transcription (RT) reaction using High Capacity RNA-to-cDNA kit (Life Technologies #4387406) following the manufacturer's instructions. Final RT products were diluted 10 folds in water and PCR reactions were performed using GoTaq Flexi DNA Polymerase (Promega #M8295). 1 μL of cDNA was added in a total volume of 25 μL containing 2 mM MgCl$_2$, 1 × PCR buffer, 0.2 mM deoxyribonucleotide triphosphates (dNTPs), 0.5 μM each of the primers (Supplementary Table 2, Integrated DNA Technology) and 0.625 unit of Taq DNA polymerase. The PCR settings for all the genes were as follows: 95 °C for 2 min, 30 cycles through 95 °C for 30 s, 59 °C for 30 s, and 72 °C for 30s, then extension at 72 °C for 5 min. Reaction for housekeeping gene *GAPDH* was run as control. 2 μL of the PCR mixture was electrophoresed on 8% Native-PAGE gel at 300 V for 1.5 h, followed by CYBER Gold (Life Technologies, #S-11494) staining and imaging with the GE Healthcare Typhoon 9400 scanner system.

2.13. Statistical analysis

Data with error bars are from at least 3 replicate experiments (except for Fig. 2a from duplicate experiments), and are presented as the mean ± standard deviation (SD). Statistical analyses were done using the statistical package Instat (GraphPad Software). The means of triplicate samples were evaluated using t-test or one-way ANOVA as indicated in the Figure legends.

3. Results and discussion

3.1. Construction and characterization of TAT-peptide coated HGN-siRNA

Efficient delivery of siRNA to hESC is known to be difficult for synthetic vectors [19]. To overcome this limitation, we designed a multi-functional nanoparticle carrier by attaching the generic cell penetrating peptide TAT (biotin-YGRKKRRQRRR) onto hollow gold nanoshells functionalized with multivalent siRNA (Fig. 1a). Multiple copies of functional siRNA molecules were conjugated to the surface of the ~50 nm diameter HGN through a quasi-covalent Au−S bond, whereas uptake of the construct by hESC was mediated by the TAT-peptide coating on the particle surface. Upon pulsed NIR laser irradiation, the HGNs strongly absorb pulsed NIR laser light, which is rapidly (nanosecond) converted to heat, ablating the Au−S bond holding the siRNA on HGN surface and producing transient vapor bubbles that ruptures the endosome without damaging the siRNA [36] or the hESC (Fig. 1a). This strategy results in the successful intracellular transfer of negatively charged siRNA to the cytosol of hESC, thereby initiating RNAi-mediated gene knockdown and stem cell differentiation.

A high number of siRNA duplexes (~2300) were conjugated to the surface of each HGN (~50 nm) through low pH-induced self-assembly of thiolated RNA sense strand followed by the hybridization of the anti-sense strand as described previously [36]. In our prior work (siRNA delivery to a mouse endothelial cell line), we modified TAT peptide with a lipid to form a lipid bilayer around the HGN-siRNA, insulating against nanoparticle−nanoparticle electrostatic coupling [35]. Adopting that strategy here generated TAT-coated HGN in a stable colloidal formulation (with an absorption peak at ~800 nm) and efficient siRNA loading (Supplementary Fig. 1), however, their internalization in hESC was not sufficient to cause effective gene silencing upon laser treatment (Supplementary Fig. 2). Due to the synthetic constraints this strategy was not amenable to testing peptide sequences or other structural variations. We then pursued an assembly strategy wherein the thiolated siRNA molecules were backfilled onto thiol-
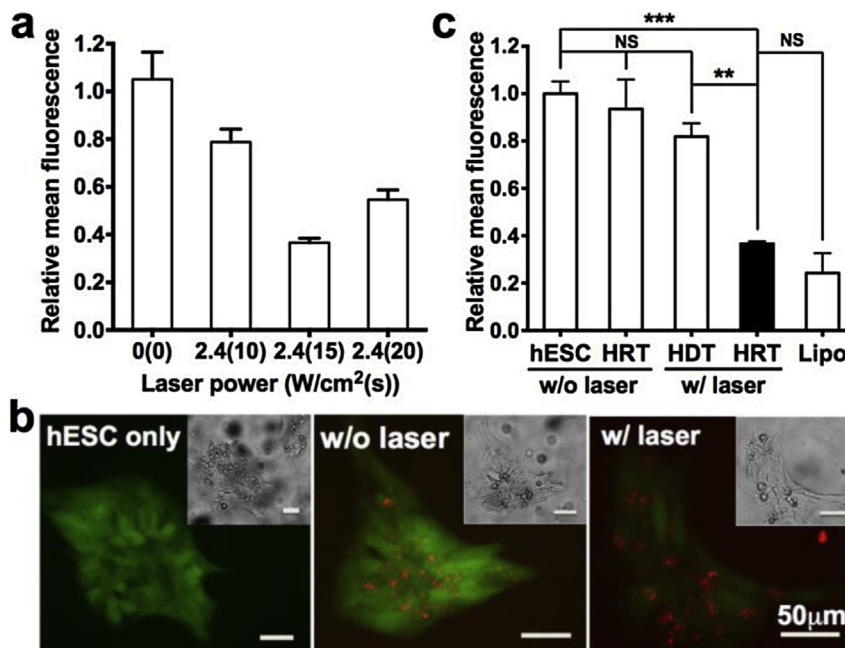
Fig. 2. GFP knockdown in H9-GFP cells via HGN-mediated GFP-siRNA delivery and NIR-laser excitation (2.4 W/cm^2 for 15 s). (a) Laser power and irradiation duration optimization for effective GFP knockdown in H9-GFP cells. Cells are assayed by flow cytometry 3 days after laser treatment. (b) Fluorescence imaging of H9-GFP cells 3 days after HRT (coated with GFP-siRNA) internalization and laser treatment. (c) Mean fluorescence intensity of cells with and without HRT and HDT (dsDNA control) and laser treatment. Cells are assayed by flow cytometry 3 days after laser treatment. Lipo: Lipofectamine RNAiMAX siRNA transfection. Data sets are analyzed by one-way ANOVA. **, p < 0.01; ***, p < 0.001; NS, not significant.

PEG5k-TAT coated HGN. The nanoparticles did not aggregate after siRNA backfilling (Supplementary Fig. 1a), and had strong internalization into hESC (Supplementary Fig. 2a), but this approach showed inefficient laser knockdown of GFP in cells, possibly due to the insufficient amount of siRNA release by laser (Supplementary Fig. 1b, Supplementary Fig. 2b).

Our optimized design places a ~5 nm streptavidin bridging element between a biotinylated RNA layer and a biotinylated TAT-peptide (Fig. 1a). The average hydrodynamic diameter of the final construct HGN-siRNA-Biotin-STV-TAT (HRT) increased from 56 for bare HGN (citrate stabilized) to 151 nm (Fig. 1b), which can be attributed to the sum of RNA length, protein/peptide coating, and slight aggregation [40]. The plasmon resonance of the nanoparticles red-shifted from ~710 nm for bare HGN to ~880 nm after the final coating step (Fig. 1b). By tracing the dye label on the siRNA [36], we found that irradiation of HRT by our pulsed NIR laser at 800 nm wavelength caused the release of ~530 siRNA duplexes per particle (~23% of capacity), at a power density of 2.4 W/cm^2 for 15 s (Supplementary Fig. 3) with 1 kHz pulse repetition rate, ~120 fs pulse duration. This streptavidin-TAT coating strategy was sufficient to cause the desired biological effect. However, future optimization could improve the HGN monodispersity that dictates the sharpness of the absorption resonance peak, and more closely match nanoparticle absorption to the wavelength of the exciting laser.

3.2. Protocol optimization and HGN-mediated GFP knockdown evaluation in transduced hESC

The compact clusters of hESC reduce accessibility to transfection; thus, protocols often rely on enzymatic digestion to generate single cells that leads to significant loss of cell viability [19]. We instead used a non-enzymatic method for the dissociation of the hESC that generated single cells and small cell aggregates (5–10 cells) while ensuring minimum cell damage, and membrane

accessibility to nanoparticles. Notably, we found that a 10 min incubation of attached hESC with Ca^{2+} and Mg^{2+} free PBS (37 °C) followed by manual dissection was sufficient for cell dissociation. Cells generated by this mild treatment appeared to take up more nanoparticles than cells obtained using commercial non-enzymatic cell dissociation buffer treatment (CDB, Invitrogen) (Supplementary Fig. 4). Crucially, addition of ROCK inhibitor within the first 24 h after single cell seeding significantly increased the cell viability (Supplementary Fig. 5). The optimized HGN transfection protocol (Supplementary Fig. 6) that we developed here enables both efficient cellular uptake and robust cell viability.

To demonstrate the NIR laser-dependent siRNA activation in hESC, as well as to optimize siRNA delivery efficiency, HGN particles carrying GFP-siRNA were incubated with GFP-expressing hESC (H9-GFP), followed by NIR laser irradiation. Nanoparticles with 6 pmol siRNA were used for 4×10^5 cells (~4000 nanoparticles per cell). A set of different laser powers was tested, and 2.4 W/cm^2 for 15 s was found to have the maximum GFP silencing effect (Fig. 2a) and was selected for later studies. Fluorescence imaging of H9-GFP cells 3 days post treatment showed that GFP expression in cells decreased significantly only when cells carrying particles were irradiated with laser (Fig. 2b).

Flow cytometry quantification of GFP fluorescence in H9-GFP cells at day 3 showed that the mean fluorescence of the whole cell population after particle internalization and laser treatment decreased by ~60% compared to cells without particle and laser treatment (Fig. 2c), consistent with the decrease (~66%) of the cell population with high GFP expression (Supplementary Fig. 7). This down-regulation efficiency is similar to the best data using commercially available transfection reagents including Lipofectamine 2000, jetPRIME, and Lipofectamine RNAiMAX (with 15 pmol siRNA for 1×10^5 cells) (Fig. 2c and Supplementary Fig. 8), but our method requires ~ ten-fold less siRNA. The knockdown efficiency of our method can be further increased by optimizing particles to release more of the siRNA load upon laser treatment, and by
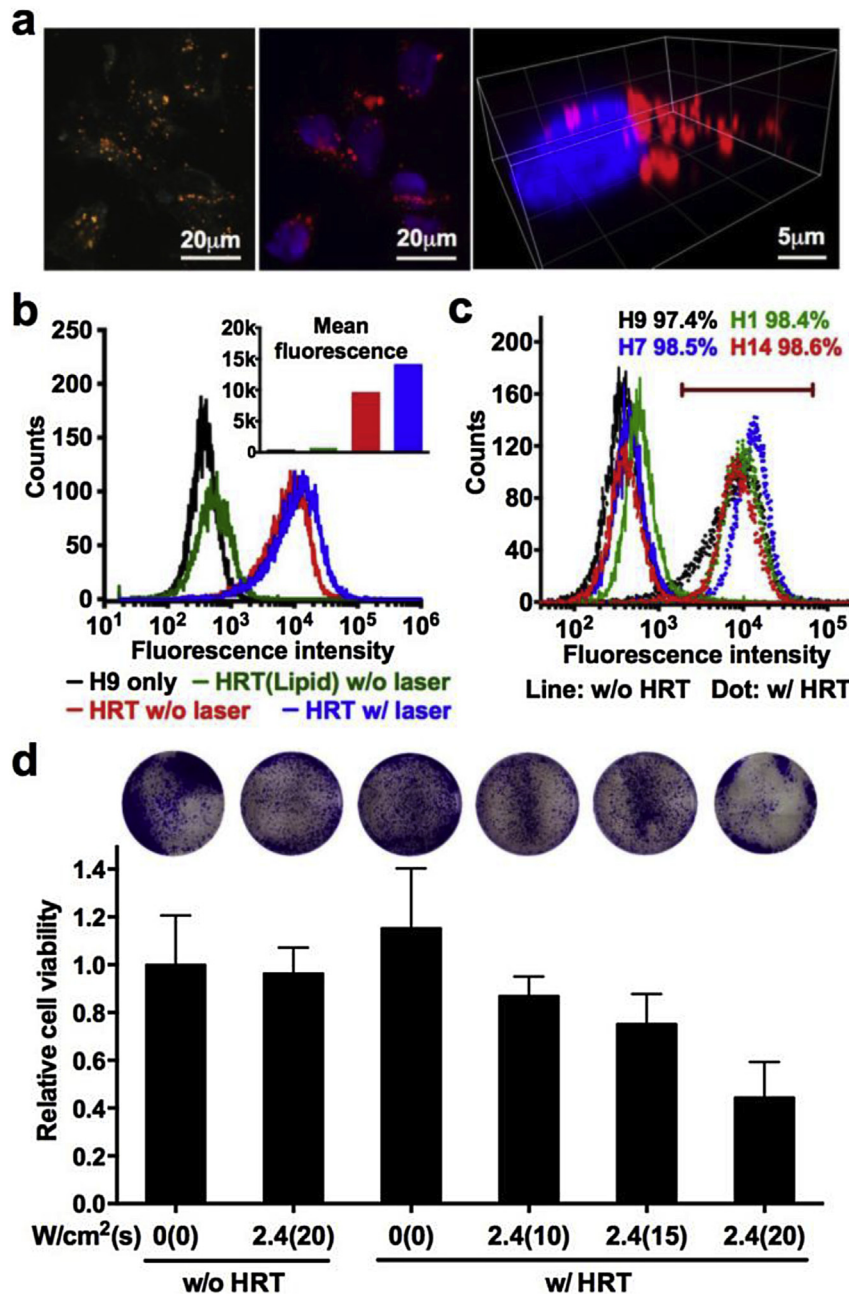
Fig. 3. Cellular uptake of HRT in un-engineered hESC and cytotoxicity assay of the particle and pulsed NIR laser treatment. (a) Microscopic visualization of particles internalized by hESC H9 cells. Left: Dark-field imaging of cells shows gold punctate dots due to HGN light scattering, which are co-localized with red fluorescent puncta (from Quasar570) surrounding the nucleus (see middle panel). Right: 3D image of a single cell by confocal fluorescence microscopy shows nanoparticles (red puncta from the fluorescent dye Quasar570) collecting around the nucleus (blue by Hoechst staining). (b) Flow cytometry quantification of particle internalization and laser release in H9 cells. HRT(Lipid): HGN-siRNA-TAT by lipid coating strategy. Top right: mean fluorescence of each peak showing increased intensity after laser treatment that indicates the release of fluorescent payload. (c) HRT is efficient (>97%) in penetrating a series of different hESC cell lines including H1, H7, H9 and H14. The bar is defined as being above the brightest 1% of the unlabeled control cells. (d) Cell viability assessment of H9 cells after internalization of HRT (with dsRNA coating non-sense to H9 cells) and treatment with different laser powers. No significant difference was observed from the t-test analysis between cells without HRT without laser and cells with HRT with laser irradiation at 2.4 W/cm² for 15 s. Top panel: cell colonies stained by crystal violet 5 days post laser treatment. (For interpretation of the references to color in this figure legend, the reader is referred to the web version of this article.)

modifying the laser irradiation protocol to illuminate the entire cell population. GFP expression remained unchanged in the controls, including cells incubated with GFP-siRNA-carrying HRT without laser irradiation, cells incubated with non-sense dsDNA-carrying HDT and with laser irradiation, and cells without nanoparticles or laser treatment (Fig. 2c). Collectively, these findings strongly suggest that down-regulation of GFP results from siRNA being released from HRT nanoparticles, and that NIR laser irradiation is necessary for such siRNA activation in the cells.

3.3. Nanoparticle internalization in un-engineered hESC and analysis of cytotoxicity

The HRT nanoparticle was then tested for the penetration into un-engineered hESC with our optimized transfection protocol (Supplementary Fig. 6). We labeled siRNA with Quasar570 to track the internalization of HRT into hESC H9 cells over a 2 h incubation at 37 °C (Fig. 1a). Dark-field microscopy of cells after nanoparticle incubation showed orange-red puncta, due to the light scattering of
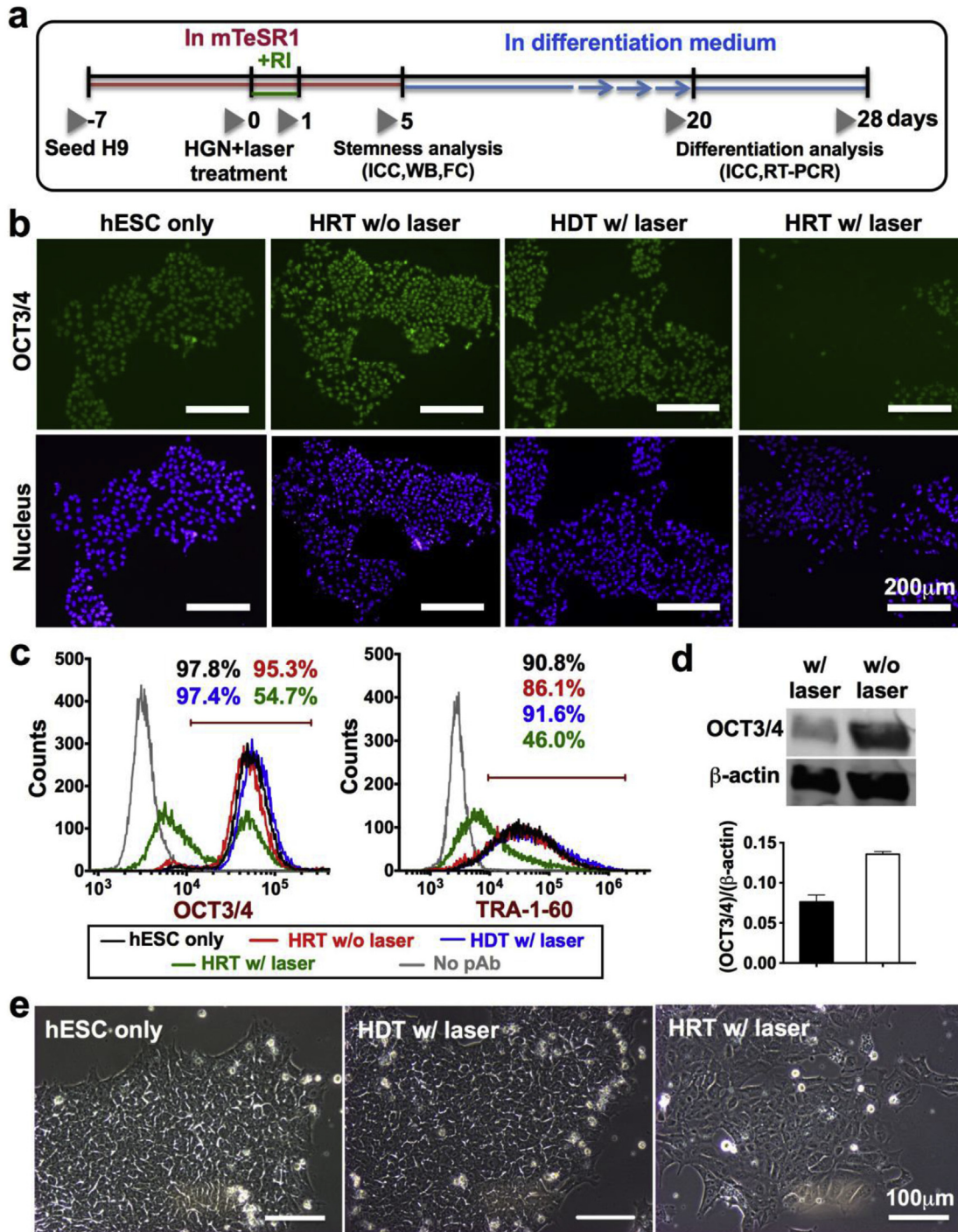
Fig. 4. Release of *Oct4*-siRNA from HRT in H9 hESC cells by NIR laser (2.4 W/cm^2 for 15 s) down-regulates OCT4 protein levels and leads to stem cell differentiation in the mTeSR1 medium. (a) Time schedule of the whole protocol and assays of particle and laser treatment to cells. (b) ICC staining of H9 5 days after particle internalization and laser treatment. (c) Flow cytometry of H9 cells stained with stem cell markers including OCT3/4 and TRA-1-60 5 days post particle and laser treatment in mTeSR1 medium, compared to the undifferentiated cells in controls (hESC only, HRT without laser and HDT with laser). Bars are defined as being above the brightest 1% of the unlabeled control cells, incubated with secondary antibody but without primary antibody. (d) Western blot analysis of OCT4 protein level in H9 cells. The bar graph underneath shows the band intensity ratio of OCT4 to β-actin in the Western blot image. (e) Morphology of cells 5 days post HRT or HDT and laser treatment (cultured in the mTeSR1 medium).

HGN, surrounding the cell nucleus and this co-localized with the red fluorescence puncta from Quasar570 (Fig. 3a). Confocal fluorescence microscopy 3D images of selected single cells confirmed the intracellular distribution of the siRNA (likely inside endosomes) near the nucleus (Fig. 3a). We quantified the cellular internalization by flow cytometry using the Quasar570 fluorescence intensity and the fluorescence change after pulsed NIR laser irradiation (Fig. 3b). Approximately 97% of the H9 cell population showed significant fluorescence due to HRT uptake, defined as being brighter than the brightest 1% of the unlabeled control cells. We observed that the mean fluorescence of the cells was increased by 44% after laser irradiation, consistent with RNA payload release (since Quasar570
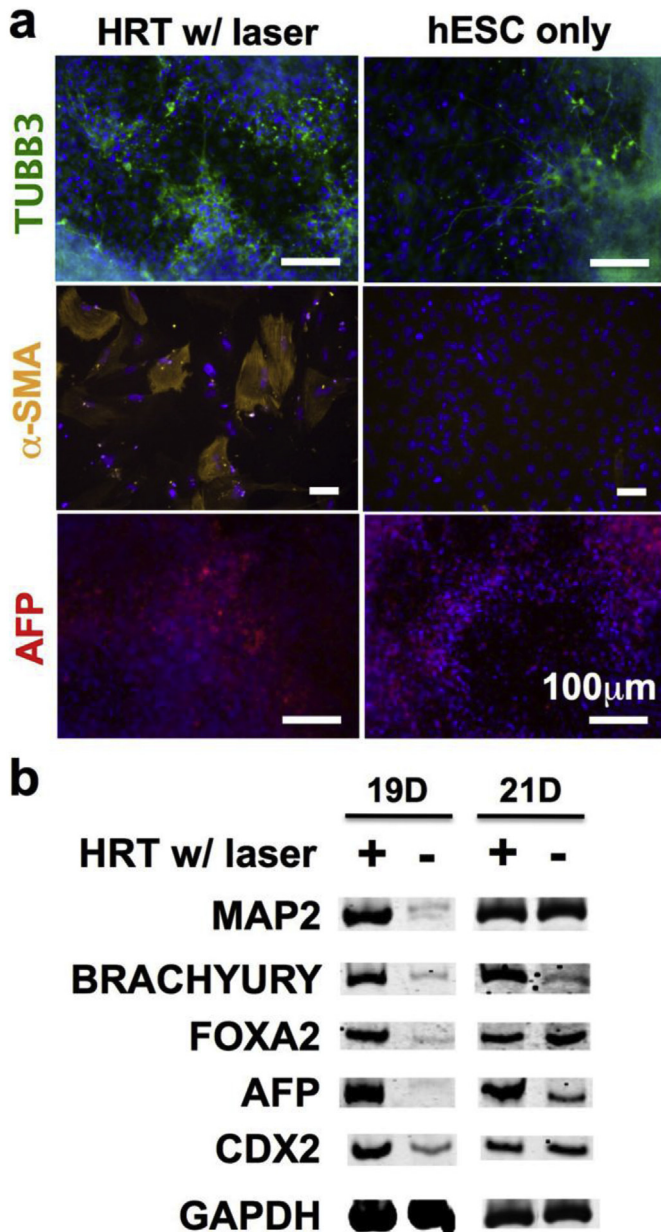
Fig. 5. The HGN and NIR laser-mediated *Oct4* gene knockdown accelerates the ability of hESC H9 cells to differentiate into all three germ layers in differentiation medium, indicated by ICC staining and RT-PCR analysis of differentiation markers. (a) ICC of βIII-tubulin (TUBB3, ectoderm marker), α-smooth muscle actin (α-SMA, mesoderm marker), and α-fetoprotein (AFP, endoderm marker) for cells 20 or 28 days (20 for α-SMA, 28 for TUBB3 and AFP) after particle and laser treatment. (b) RT-PCR analysis of differentiation biomarkers in H9 cells 19 and 21 days after particle and laser treatment. MAP2: ectoderm; BRACHYURY: mesoderm; FOXA2, AFP, CDX2: endoderm.

is partially quenched when near the gold surface [41]). Importantly, HRT showed similar high internalization efficiency (>97%) across a series of hESC cell lines including H1, H7 and H14 (Fig. 3c).

To assess any effect from particles and laser treatment to cell viability, H9 cells containing HRT with double-stranded RNA (nonsense to H9 cells) were exposed to NIR laser of different powers, and cultured on Matrigel-coated plates for 5 days. Live cells growing on the plate were stained with crystal violet, while dead cells that had lost the ability to attach were washed during fresh medium exchange every other day [42,43]. Fig. 3d shows that the laser irradiation with power and time at or below 2.4 W/cm^2 for

15 s had no significant impairment on cell viability, compared to untreated control cells. Cell stemness was also not affected, judging by cell morphology 7 days after particle and laser treatment (2.4 W/cm^2 for 15 s), since it was normal for untreated cells to have large nuclei and be tightly packed to form colonies with smooth edges (Supplementary Fig. 9) [44]. Importantly, since the expression levels across a panel of stem cell biomarkers was not changed after laser irradiation of cells loaded with HDT, which carries a control double-strand DNA (non-sense to H9), we conclude that specific stemness changes can only be related to the RNA activity, not the effects of the laser, gold, streptavidin, or peptide.

3.4. Light-activated Oct4 knockdown in hESC accelerates stem cell differentiation

Inspired by the success of HGN-siRNA delivery in H9-GFP cells described above, we next set out to deliver siRNA to the original unengineered H9 cells to down-regulate a gene with biological activity and investigate the biological outcomes. We chose to target the expression of the *Oct4* gene, which is an essential transcription factor for embryonic stem cell self-renewal and pluripotency [45]. The down-regulation of this protein was reported to initiate and accelerate differentiation [45]. We first tested the siRNA knockdown of the *Oct4* gene in H9 cells using a lentiviral transfection method with the plasmid LL-OCT4-1/2 (Addgene) (Supplementary Fig. 10). The down-regulation of *Oct4* expression in hESC H9 cells by this means initiated the differentiation process in the mTeSR1 medium (control was only barely differentiated) (Supplementary Fig. 10b) and accelerated this process in the differentiation medium (control was slower) (Supplementary Fig. 10c). The cells stained positive for all three germ layer markers after extended culture in the differentiation medium (Supplementary Fig. 10c). In parallel, we incubated H9 cells with our HRT construct HGN-siRNA(*Oct4*)-TAT and treated them with the NIR pulsed laser at 2.4 W/cm^2 for 15 s optimized from H9-GFP knockdown experiment and cell viability test, followed by cell assays after 5 days culture in mTeSR1 medium to get enough cells (Fig. 4a). These conditions stimulated *Oct4*-siRNA function, as demonstrated by a significant decrease of OCT4 protein expression level at day 5 confirmed by immunocytochemistry (ICC) staining and Western blot assay (Fig. 4b–d). Flow cytometry quantification at day 5 (cells cultured in mTeSR1 medium) showed that ~50% of the cell population had decreased their expression of stem cell markers including OCT3/4 and TRA-1-60, as evidence of cell differentiation (Fig. 4c). Limited by cell number, our analysis of the knockdown and differentiation assay carried on day 5 might be an underestimation of the true knockdown efficiency since we noticed that undifferentiated cells divide more quickly than differentiated cells in mTeSR1 medium.

Fig. 4e and Supplementary Fig. 11 show that cells cultured with HRT and exposed to laser treatment exhibited differentiated cell characteristics: enlarged cell size, increased cytoplasmic area with decreased nuclear-to-cytoplasmic ratio. Consistent with the GFP knockdown experiments, laser exposure of HRT was required for the knockdown effect. Cells treated with HDT (HGN-dsDNA-TAT carrying non-sense dsDNA) did not show any apparent downregulation of OCT4 protein, loss of stem cell markers or stem cell morphology change (Fig. 4c,e), supporting that the particle internalization and laser treatment themselves have no side effects on cell stemness. Together, the results confirm that the downregulation of *Oct4* gene in H9 cells by this strategy leads to stem cell differentiation in a NIR laser-dependent manner.

As laser-induced siRNA delivery in hESC has not been explored previously, we investigated whether this method might cause cell differentiation to be biased toward certain germ layers. Cells were siRNA-treated (Fig. 4a) and then assayed from day 20–28 by ICC

staining of three germ layer biomarkers including βIII-tubulin (TUBB3, for ectoderm), α-smooth muscle actin (α-SMA, for mesoderm) and α-fetoprotein (AFP, for endoderm), and reverse transcription PCR (RT-PCR) analysis of several biomarkers' mRNA expression. Note that after the particle and laser treatment, the cells were switched to the differentiation medium to avoid the overwhelming growth of undifferentiated cells in mTeSR1 medium, then further cultured and assayed. Consistent with our observation from lentiviral Oct4 knockdown, HGN- and laser-dependent Oct4 knockdown accelerated the differentiation process compared to untreated self-differentiation in differentiation medium, as indicated by biomarker ICC staining and RT-PCR analysis (Fig. 5). H9 cells without particle and laser treatment (but with the same culture protocol) showed a delay, with α-SMA expression at day 28 (Fig. 5a and Supplementary Fig. 12), and apparently lower expression of TUBB3 and AFP at day 28, as compared to cells with particle and laser treatment (Fig. 5a). RT-PCR analysis of biomarkers for all three germ layers confirms the delay at the mRNA level of untreated cells (Fig. 5b). Importantly, both ICC and RT-PCR analysis demonstrate that treatment using HRT and NIR laser does not change the ability of H9 cells to differentiate into all three germ layers (Fig. 5).

4. Conclusions

In summary, we have successfully developed a strategy to control RNAi in human embryonic stem cells using a near-infrared laser. To achieve efficient uptake we developed a new modular design for hollow gold nanoshells (HGN) that couples a targeting peptide to the siRNA. The nanoparticles each carry thousands of siRNA molecules and a streptavidin capsid, which when combined with the TAT-peptide, efficiently penetrated into a broad range of hESC including H1, H7, H9 and H14. Internalization of the constructs was tracked and quantified by flow cytometry. Exposure to femtosecond pulses of NIR light caused GFP and Oct4 knockdown in hESC, and differentiation to all three germ layers, supporting the biocompatibility of this novel method. This strategy enables laser printing of siRNA in stem cells with cellular-level resolution at a desired time, and will hence offer new avenues in stem cell basic research and stem cell tissue engineering for regenerative medicine, for example as a tool to probe effects on tissue development.

Appendix A. Supplementary data

Supplementary data related to this article can be found at http://dx.doi.org/10.1016/j.biomaterials.2015.06.006.

References

[1] J.A. Thomson, J. Itskovitz-Eldor, S.S. Shapiro, M.A. Waknitz, J.J. Swiergiel, V.S. Marshall, et al., Embryonic stem cell lines derived from human blastocysts, Science 282 (5391) (1998) 1145–1147.
[2] A.G. Smith, Embryo-derived stem cells: of mice and men, Annu. Rev. Cell. Dev. Biol. 17 (2001) 435–462.
[3] T. Enver, S. Soneji, C. Joshi, J. Brown, F. Iborra, T. Orntoft, et al., Cellular differentiation hierarchies in normal and culture-adapted human embryonic stem cells, Hum. Mol. Genet. 14 (21) (2005) 3129–3140.
[4] A. Eguchi, B.R. Meade, Y.-C. Chang, C.T. Fredrickson, K. Willert, N. Puri, et al., Efficient siRNA delivery into primary cells by a peptide transduction domain–dsRNA binding domain fusion protein, Nat. Biotechnol. 27 (6) (2009) 567–571.
[5] W.W.Y. Yau, P-o Rujitanaroj, L. Lam, S.Y. Chew, Directing stem cell fate by controlled RNA interference, Biomaterials 33 (9) (2012) 2608–2628.
[6] A. Heidersbach, A. Gaspar-Maia, M.T. McManus, M. Ramalho-Santos, RNA interference in embryonic stem cells and the prospects for future therapies, Gene Ther. 13 (6) (2006) 478–486.
[7] L. Ding, F. Buchholz, RNAi in embryonic stem cells, Stem Cell. Rev. 2 (1) (2006) 11–18.
[8] H.-J. Park, J. Shin, J. Kim, S.-W. Cho, Nonviral delivery for reprogramming to pluripotency and differentiation, Arch. Pharmacal. Res. 37 (1) (2014) 107–119.
[9] F.B. Rassouli, M.M. Matin, Gene silencing in human embryonic stem cells by RNA interference, Biochem. Biophys. Res. Commun. 390 (4) (2009) 1106–1110.
[10] B. Shah, P.T. Yin, S. Ghoshal, K.B. Lee, Multimodal magnetic core–shell nanoparticles for effective stem-cell differentiation and imaging, Angew. Chem. 125 (24) (2013) 6310–6315.
[11] A. Solanki, S. Shah, P.T. Yin, K.-B. Lee, Nanotopography-mediated reverse uptake for siRNA delivery into neural stem cells to enhance neuronal differentiation, Sci. reports 3 (2013) 1553.
[12] L. Ferreira, J.M. Karp, L. Nobre, R. Langer, New opportunities: The use of Nanotechnologies to manipulate and track stem cells, Cell. Stem Cell. 3 (2) (2008) 136–146.
[13] Y. Ma, A. Ramezani, R. Lewis, R.G. Hawley, J.A. Thomson, High-level sustained transgene expression in human embryonic stem cells using lentiviral vectors, Stem Cells 21 (1) (2003) 111–117.
[14] X.Y. Zhang, V.F. La Russa, L. Bao, J. Kolls, P. Schwarzenberger, J. Reiser, Lentiviral vectors for sustained transgene expression in human bone marrow-derived stromal cells, Mol. Ther. 5 (5) (2002) 555–565.
[15] C.E. Thomas, A. Ehrhardt, M.A. Kay, Progress and problems with the use of viral vectors for gene therapy, Nat. Rev. Genet. 4 (5) (2003) 346–358.
[16] P. Seth, Vector-mediated cancer gene therapy – an overview, Cancer Biol. Ther. 4 (5) (2005) 512–517.
[17] D.W. Pack, A.S. Hoffman, S. Pun, P.S. Stayton, Design and development of polymers for gene delivery, Nat. Rev. Drug Discov. 4 (7) (2005) 581–593.
[18] M. Zhao, H. Yang, X.J. Jiang, W. Zhou, B. Zhu, Y. Zeng, et al., Lipofectamine RNAiMAX: An efficient siRNA transfection reagent in human embryonic stem cells, Mol. Biotechnol. 40 (1) (2008) 19–26.
[19] Y. Ma, Y. Jin, C. Dong, E.C. Cheng, H. Lin, Y. Huang, et al., High-efficiency siRNA-based gene knockdown in human embryonic stem cells, RNA 16 (12) (2010) 2564–2569.
[20] Y. Omidi, J. Barar, S. Akhtar, Toxicogenomics of cationic lipid-based vectors for gene therapy: impact of microarray technology, Curr. Drug Deliv. 2 (4) (2005) 429–441.
[21] Y. Omidi, J. Barar, H.R. Heidari, S. Ahmadian, H.A. Yazdi, S. Akhtar, Microarray analysis of the toxicogenomics and the genotoxic potential of a cationic lipid-based gene delivery nanosystem in human alveolar epithelial a549 cells, Toxicol. Mech. Methods 18 (4) (2008) 369–378.
[22] O. Qutachi, K.M. Shakesheff, L.D. Buttery, Delivery of definable number of drug or growth factor loaded poly (dl-lactic acid-co-glycolic acid) microparticles within human embryonic stem cell derived aggregates, J. Control Release 168 (1) (2013) 18–27.
[23] S-h Hsu, G.-S. Huang, T.-T. Ho, F. Feng, Efficient Gene Silencing in Mesenchymal Stem Cells by Substrate-Mediated RNA Interference, Tissue Eng. Part C. Methods 20 (11) (2014) 916–930.
[24] S. Shah, P.T. Yin, T.M. Uehara, S.T.D. Chueng, L. Yang, K.B. Lee, Guiding stem cell differentiation into oligodendrocytes using graphene-nanofiber hybrid scaffolds, Adv. Mater. 26 (22) (2014) 3673–3680.
[25] M.K. Nguyen, O. Jeon, M.D. Krebs, D. Schapira, E. Alsberg, Sustained localized presentation of RNA interfering molecules from in situ forming hydrogels to guide stem cell osteogenic differentiation, Biomaterials 35 (24) (2014) 6278–6286.
[26] L.H. Peng, J. Niu, C.Z. Zhang, W. Yu, J.H. Wu, Y.H. Shan, et al., TAT conjugated cationic noble metal nanoparticles for gene delivery to epidermal stem cells, Biomaterials 35 (21) (2014) 5605–5618.

[27] J. Zoldan, A.K. Lytton-Jean, E.D. Karagiannis, K. Deiorio-Haggar, L.M. Bellan, R. Langer, et al., Directing human embryonic stem cell differentiation by non-viral delivery of siRNA in 3D culture, Biomaterials 32 (31) (2011) 7793—7800.

[28] S.F. Badylak, D. Taylor, K. Uygun, Whole-organ tissue engineering: decellularization and recellularization of three-dimensional matrix scaffolds, Annu. Rev. Biomed. Eng. 13 (2011) 27—53.

[29] N. Gjorevski, A. Ranga, M.P. Lutolf, Bioengineering approaches to guide stem cell-based organogenesis, Development 141 (9) (2014) 1794—1804.

[30] B.G. Prevo, S.A. Esakoff, A. Mikhailovsky, J.A. Zasadzinski, Scalable routes to gold nanoshells with tunable sizes and response to near-infrared pulsed-laser irradiation, Small 4 (8) (2008) 1183—1195.

[31] T. Nakano, S. Ando, N. Takata, M. Kawada, K. Muguruma, K. Sekiguchi, et al., Self-formation of optic cups and storable stratified neural retina from human ESCS, Cell. Stem Cell. 10 (6) (2012) 771—785.

[32] Y. Sasai, Cytosystems dynamics in self-organization of tissue architecture, Nature 493 (7432) (2013) 318—326.

[33] H. Suga, T. Kadoshima, M. Minaguchi, M. Ohgushi, M. Soen, T. Nakano, et al., Self-formation of functional adenohypophysis in three-dimensional culture, Nature 480 (7375) (2011) 57—62.

[34] E. Ikeda, R. Morita, K. Nakao, K. Ishida, T. Nakamura, T. Takano-Yamamoto, et al., Fully functional bioengineered tooth replacement as an organ replacement therapy, Proc. Natl. Acad. Sci. U. S. A. 106 (32) (2009) 13475—13480.

[35] G.B. Braun, A. Pallaoro, G.H. Wu, D. Missirlis, J.A. Zasadzinski, M. Tirrell, et al., Laser-activated gene silencing via gold nanoshell-siRNA conjugates, ACS Nano 3 (7) (2009) 2007—2015.

[36] X. Huang, A. Pallaoro, G.B. Braun, D.P. Morales, M.O. Ogunyankin, J. Zasadzinski, et al., Modular plasmonic nanocarriers for efficient and targeted delivery of cancer-therapeutic siRNA, Nano Lett. 14 (4) (2014) 2046—2051.

[37] E.Y. Lukianova-Hleb, A. Belyanin, S. Kashinath, X.W. Wu, D.O. Lapotko, Plasmonic nanobubble-enhanced endosomal escape processes for selective and guided intracellular delivery of chemotherapy to drug-resistant cancer cells, Biomaterials 33 (6) (2012) 1821—1826.

[38] B.R. Meade, S.F. Dowdy, Enhancing the cellular uptake of siRNA duplexes following noncovalent packaging with protein transduction domain peptides, Adv. Drug Deliv. Rev. 60 (4—5) (2008) 530—536.

[39] J.J. Turner, S. Jones, M.M. Fabani, G. Ivanova, A.A. Arzumanov, M.J. Gait, RNA targeting with peptide conjugates of oligonucleotides, siRNA and PNA, Blood Cells Mol. Dis. 38 (1) (2007) 1—7.

[40] K.Y. Win, S.S. Feng, Effects of particle size and surface coating on cellular uptake of polymeric nanoparticles for oral delivery of anticancer drugs, Biomaterials 26 (15) (2005) 2713—2722.

[41] P.C. Ray, A. Fortner, G.K. Darbha, Gold nanoparticle based FRET asssay for the detection of DNA cleavage, J. Phys. Chem. B 110 (42) (2006) 20745—20748.

[42] Y. He, J.W. Zhou, L. Xu, M.J. Gong, T.C. He, Y. Bi, Comparison of proliferation and differentiation potential between mouse primary hepatocytes and embryonic hepatic progenitor cells in vitro, Int. J. Mol. Med. 32 (2) (2013) 476—484.

[43] E.Y. Huang, Y. Bi, W. Jiang, X.J. Luo, K. Yang, J.L. Gao, et al., Conditionally Immortalized Mouse Embryonic Fibroblasts Retain Proliferative Activity without Compromising Multipotent Differentiation Potential, PLoS One 7 (2) (2012) e32428.

[44] H. Sathananthan, M. Pera, A. Trounson, The fine structure of human embryonic stem cells, Reprod. Biomed. Online 4 (1) (2002) 56—61.

[45] G.J. Pan, Z.Y. Chang, H.R. Scholer, D.Q. Pei, Stem cell pluripotency and transcription factor Oct4, Cell. Res. 12 (5—6) (2002) 321—329.